



HAL
open science

Numerical and experimental study of the International Space Station crew quarters ventilation

Matei Razvan Georgescu, Amina Meslem, Ilinca Nastase, Mihnea Sandu

► **To cite this version:**

Matei Razvan Georgescu, Amina Meslem, Ilinca Nastase, Mihnea Sandu. Numerical and experimental study of the International Space Station crew quarters ventilation. *Journal of Building Engineering*, 2021, 41, pp.102714. 10.1016/j.jobe.2021.102714 . hal-03263171

HAL Id: hal-03263171

<https://univ-rennes.hal.science/hal-03263171>

Submitted on 17 Jun 2021

HAL is a multi-disciplinary open access archive for the deposit and dissemination of scientific research documents, whether they are published or not. The documents may come from teaching and research institutions in France or abroad, or from public or private research centers.

L'archive ouverte pluridisciplinaire **HAL**, est destinée au dépôt et à la diffusion de documents scientifiques de niveau recherche, publiés ou non, émanant des établissements d'enseignement et de recherche français ou étrangers, des laboratoires publics ou privés.

Matei-Razvan GEORGESCU: Methodology, Formal analysis, Investigation, Writing – Original Draft, Visualization. **Amina MESLEM:** Conceptualization, Writing – Review & Editing, Supervision, Funding acquisition. **Ilinca NASTASE:** Conceptualization, Resources, Writing – Review & Editing, Supervision, Funding acquisition. **Mihnea SANDU:** Methodology, Investigation, Resources, Writing – Original Draft.

Journal Pre-proof

Numerical and Experimental Study of the International Space Station Crew Quarters Ventilation

Corresponding author: Matei Razvan GEORGESCU^{1,2*}

mateirazvangeorgescu@gmail.com

matei-razvan.georgescu@etudiant.univ-rennes1.fr

Phone: +40724818295

Fax number: +40212420781

Postal address: 66 Pache Protopopescu, 021414, Bucharest, Romania

Amina MESLEM¹

amina.meslem@univ-rennes1.fr

Ilinca NASTASE²

ilince.nastase@utcb.ro

Mihnea SANDU²

mihnea.sandu@utcb.ro

¹LGCGM, University of Rennes, 3 Rue du Clos Courtel, BP 90422; 35704 Rennes CEDEX 7, France

²CAMBI Research Centre, Technical University of Civil Engineering of Bucharest, 66 Pache Protopopescu boulevard, Postal code: 021414, Bucharest, Romania

Abstract

The current paper proposes a detailed study of the ventilation system of the crew quarters (CQ) aboard the International Space Station (ISS) in order to identify the ventilation system's capacity to reduce CO₂ accumulation around an occupant. These results would enable the improvement of the ventilation system, thereby decreasing the health risks of the occupants. The ventilation flow fields are studied through numerical results which are validated with experimental Particle Image Velocimetry (PIV) measurements in a reduced-scale mock-up. The equivalence between the reduced scale experimental and the full-scale numerical results is obtained through a Reynolds-number based similitude criteria. This enabled the authors to validate the isothermal airflow in the full-scale numerical model with the experimental results of the water flow in the reduced-scale mock-up. Normalized numerical and experimental velocity profiles have been superposed and were found to be in good agreement. Both numerical and experimental models highlight a stagnation region in the centre of the CQ volume leading to a ventilation deficit of the astronaut's breathing zone. The results indicate that this stagnant region is a reason for the excess CO₂ accumulation in the CQ, despite the high ventilation rate (>45 hourly air exchanges). To the author's best knowledge this is the first numerical study of the CQ ventilation system validated with reduced-scale experimental modelling. The paper's findings have implications in building air quality studies, suggesting that targeted ventilation is preferable to raw increased in flow rates.

Keywords: ISS ventilation, PIV measurements, Fan operating curve, Similitude study.

1. Introduction

There are currently four personal cabins called Crew Quarters (CQ) that are installed on the International Space Station (ISS) in the Harmony node area. The role of the CQ is to provide an acoustically quiet and visually isolated area in which crew members can sleep, relax, and retreat to a private zone. The crew uses the CQ primarily for sleeping, but also for performing tasks such as putting on or removing clothing, private communication, and personal hygiene. Each CQ was designed with noise control solutions, laptop and internet connections to allow crew members personal communication with family and friends.

Each CQ is equipped with an individual ventilation system aiming to ensure acceptable air quality in the CQ volume. Its primary role is to remove Carbon Dioxide (CO₂), which is categorized as a catastrophic hazard (danger of asphyxiation) [1–3]. Carbon dioxide, a natural product of human metabolism, accumulates quickly in sealed environments when humans are present, and can induce headaches, among other symptoms. Major resources are expended to control CO₂ levels to concentrations that are tolerable to the crews of spacecraft that are usually much higher than the ones found on Earth [1,4–6]. As NASA looks ahead to long-duration missions conducted far from Earth [7], difficult issues arise related to the management and effects of human exposure to CO₂. One is the problem of "pockets" of CO₂ in the habitat caused by excess generation of the gas in one location without a mechanism to flush the area with fresh air.

The ventilation system of each CQ is composed of two axial fans placed inside a ducting system, with intake, inlet and outlet grilles. The presence of two fans ensure safety in the event one of the fans should fail. Despite the fans having a variable flow rate [8,9] and the fact that the inlet diffuser has adjustable vanes allowing a certain degree of orientation for the air flow, different ISS reports [4,8,9] indicate that there could be situations where the CQ ventilation system is unable to fulfil air quality requirements. This fact justifies the present work.

The CQ ventilation system settings were designed experimentally on Earth, previous to the CQ's deployment to the ISS [10]. The two axial fans of the ventilation system are provided with a controller allowing the occupant of the CQ to vary the air flow rate. The air flow rate interval is 96 - 162 m³/h (corresponding to 45-77 hourly air exchanges). For practical safety and maintenance purposes, the controller of the ventilation system allows the fans to operate at three different speeds corresponding to three values of the volumetric flow rate, respectively: 108, 138 and 156 m³/h. It was found during preliminary measurements that the two thirds of the inner volume display average velocity values between 0.051-0.23 m/s fulfilling the design criteria of interior uniform flow in the CQ. However, one must note here that the corresponding experimental velocity fields are not available in the literature. The given velocity values (in the range of 0.051-0.23 m/s) [10] were probably obtained using a punctual portable thermo-anemometer, which can only provide indications of velocity levels, without providing a global view of the flow in the cabin and its interaction with the occupant. During these experiments on Earth, the noise level in the cabin exceeded the NC-40 curve by 3-5 dB at frequencies between 250 - 750 Hz [8,10].

Since the deployment of the CQs on the ISS in 2008, crew feedback has been reported relating to the CQ cabins [9]. In general, reports state that the variable fan speed and the diffuser grille provided acceptable adjustability. However, most crew members set the diffuser grille to direct air in one direction and leave it in that position, never using its orientability. The chosen fan speed varied from person to person, but most crew members reported that the fans were kept on medium or high speed for most of the time. The lowest fan flow rate (108 m³/h) occasionally results in a fan alarm going off [8,9]. These caution alarms are related to a decrease in airflow inside the cabin environment (risking an increase in CO₂ levels), attributed to dust accumulation in the ventilation ducts which introduces head losses, thereby reducing the flow rate and triggering the alarm. As the velocity design criteria for uniform flow inside the CQ (i.e., a mean velocity in the range of 0.051-0.23 m/s) are already low and since they were evaluated during the design phase of the CQ, it is safe to assume that no dust had yet accumulated in the ducts and thus they represent a best-case scenario.

Insufficient ventilation (due either to low flow rate or poor air diffusion) results in the crew rebreathing CO₂ from their exhaled breath, exposing them to a much higher concentration of CO₂ than out of breathing zone

measurements would suggest. Another issue is presented by inter-individual differences in the susceptibility of crew members to CO₂ exposure. Anecdotal reports from the International Space Station (ISS) crews suggest that certain individuals may experience a greater susceptibility to CO₂ [2,4,11].

One can question the concept that having two-thirds of the CQ volume with velocities in the 0.051 – 0.23 m/s range ensures sufficient air renewal in all points of the cabin. In fact, it can be counterproductive since the CO₂ accumulation is not uniform volume-wide, but localized. In the present authors opinion, ventilation should be targeted on the localized CO₂ pockets which form in poorly ventilated regions.

Identifying these regions implies a study of the flow field in the entire volume of the CQ. Generally, the study of the air distribution in buildings and other occupied spaces greatly relies on the recent numerical developments. In such cases the experimental validation of the flows is of great importance, knowing the complexity of the interaction between the ventilation and the irregular geometries of the surfaces for instance. One ideal case would be the one in which the numerical and experimental the flow fields could be compared in their integrality. However, most of the time researchers must contend themselves to comparing some regions of interest of the analyzed spaces. Obtaining flow fields using Particle Image Velocimetry (PIV) from a full-scale CQ model is impossible due to constructive constraints (lack of physical space inside the CQ, no transparent surface through which to capture the PIV flow fields). The authors' research team uses optical methods such as Particle Image Velocimetry (PIV) in one of our research directions, dedicated to the use of reduced scale physical models [12,13], allowing to work easily with such type of measurement tools that would allow for adapted dimensions of the region of interest to obtain high resolution velocity fields [14–17]. This type of approach must, however, comply with certain conditions of similarity.

The principles of similitude theory have applications in every domain that can benefit from reduced-scale modelling (civil engineering, wind engineering, aerospace design etc.) [18–21]. However, there are few studies based on small scale modeling applied to ventilation in buildings, and most of them are usually dedicated to natural ventilation [14,15,17,22]. Some studies [14,15,17] use water as the working fluid in the reduced scale model and base the similitude study on the Reynolds number (equivalence of Re between full-scale and reduced-scale). Among the reasons for using water as the working fluid are the small reflective particles that can be seeded in the water flow, giving higher resolution PIV measurements, but more importantly, because of the mathematics required in obtaining equivalent Reynolds numbers between the models – i.e., to keep Reynolds identical between the models, if the length scale is reduced and the fluid does not change, the velocity must be increased proportionally to the decrease in scale. By switching to water in the reduced scale from air in the full scale the difference in viscosity helps keep velocity values within obtainable limits. An evaluation of similitude methods [21] reinforces the idea that water can be used as a medium in the reduced scale and recommends the use of Reynolds as a similitude criteria where complete similarity is unobtainable and turbulent flow features are important. Given all these advantages, we decided to use water as the working fluid in this study that uses reduced scale modelling for the experimental validation.

As mentioned before, there is no detailed representation of the airflow inside the CQ up to our project, since previous CQ models used the numerical resources available at the time of their conception (2008) [6] and the subsequent on-orbit monitoring [8] used typical ultra-portable punctual measuring methods. The scientific aim of this paper is to validate a CFD numerical solution of the ISS CQ ventilation system (at 1:1 scale). The experimental validation of the numerical general ventilation flow will be based on PIV measurements in water, in a reduced scale (1:4) acrylic model of the CQ. Physical reduced scale modelling [22–24] criteria will be evaluated, with the similitude study being based on the criteria that best fits the full-scale model's conditions.

Optimization of the ventilation system presently in place to improve the quality of the air breathed by astronauts should result from easy to implement technical modifications. The authors' previous study [25] validated another essential component of our modelling approach, namely the numerical representation of the human breathing from the point of view of the breathing influenced zone and of the CO₂ accumulation. In connection to the present

paper, which aims to identify weakly ventilated regions inside the CQ, would allow the authors to identify which areas need to be targeted by the ventilation solution in order to improve the quality of the air inhaled by the ISS crew.

Thus, the objective of the present study is firstly to demonstrate the feasibility of applying reduced scale modeling for the study of ventilation systems in buildings even for complex configurations such as the confined cabin, in the presence of a human body model and secondly to allow the construction of a numerical model with robust validation will enable its subsequent use for parametric investigation and optimization. The methods presented in this study are applicable to studies concerning indoor air quality, since ventilation solutions supplying fresh air directly to the occupant's breathing zone are an increasingly important subject.

2. Theory

The outline of the experimental and numerical procedures is described by the flowchart in Figure 1. This chapter is divided in two sections: Section 1.1 – describing the theoretical considerations regarding the similitude between two models at different scales; and Section 1.2 - focused on the experimental measurement of fan operating curves, with the aim of using them as boundary conditions in the numerical models.

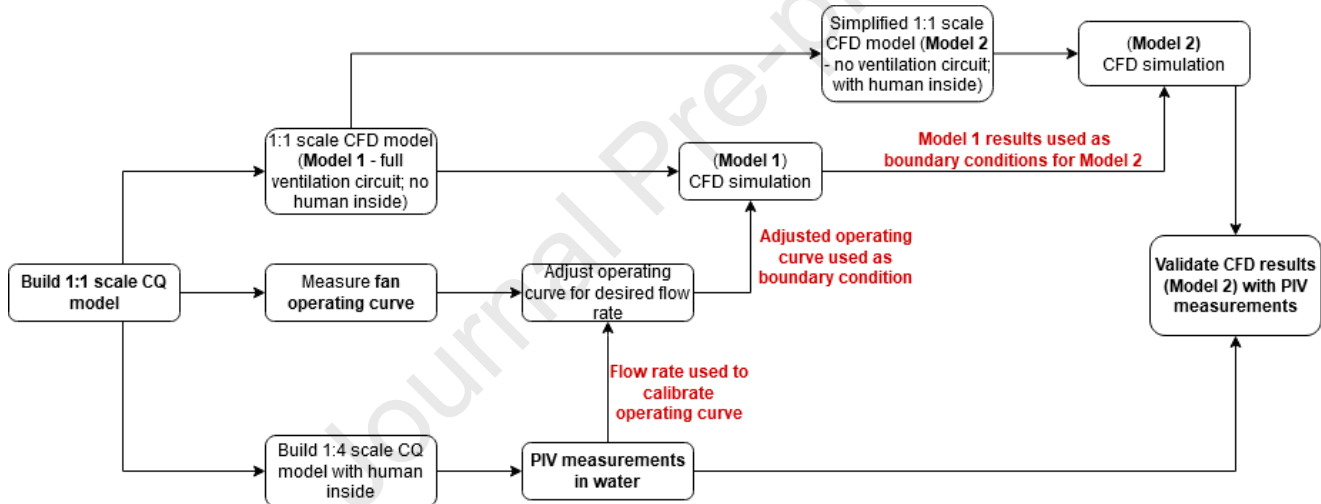


Figure 1 Flow chart of the experimental and numerical model design process and the research methodology of the paper.

2.1. Similitude study for designing the reduced scale CQ model

To validate the numerical model aiming to reproduce the general ventilation inside the CQ, detailed experimental flow distribution in the CQ is needed. The best way to acquire these fields with a satisfactory spatial resolution in a reasonable time-frame is via laser-based optical methods, which require either sufficient space, or transparency of the walls. Neither characteristics are available in the 1:1 CQ mock-up (Figure 2a). For this reason, a transparent reduced scale mock-up was developed allowing the use of optical methods. The reduced nature of the mock-up allows high spatial resolution of the velocity fields. Water was the preferred working fluid, for higher tracer resolution and the possibility of using fluorescent tracers. The use of a reduced mock-up with a different fluid requires satisfying certain similarity criteria.

In order for the results of the reduced scale model to be applicable in its full-scale equivalent, the so called similitude theory must be applied [26]. To have complete similarity between two physical phenomena, they should be of the same nature and all geometric, dynamic, kinematic similarity and boundary conditions must be achieved [26–28]. Geometric similarity implies the proportional correspondence between lengths and the equality of angles. Kinematic similarity demands that if the flow is made of particles, the corresponding particles take the same place

inside the flow pattern at the same moments in time. Lastly, dynamic similarity is required in addition to the geometric and kinematic similarity to ensure that the forces present in the model (i.e., viscous or inertial forces) have the same relative importance between the two models [27,28].

Complete similarity is the best way to ensure the replicability of the full-scale phenomena on a small-scale model but sometimes it is impossible to obtain [18,26]. In such cases phenomenological similarity must be thoroughly verified [26].

The main similarity criteria which can be considered are: Reynolds number (Re - the ratio between inertia and viscosity forces), Froude number (Fr - the ratio between inertia and gravity forces), Euler number (Eu - the ratio between inertia and pressure forces), Peclet number (Pe – related to diffusivity forces) and Schmidt number (Sc - the ratio between the intensity of substance transfer caused by pressure or concentration differences). These criteria cannot always be simultaneously satisfied and so a relevant criterion must be chosen as the basis of the similitude study. In our case, the physical models would only reproduce the flow pattern inside the CQ without buoyancy effect (the manikin is not heated and the ventilating jet as well as cabin thermal conditions are isothermal) so Fr does not significantly affect the flow fields. There are no significant pressure or concentration gradients in the experimental model (it uses only water as a fluid) so Sc is also not applicable. Pe is of lesser impact since diffusivity forces are low in comparison to inertia forces in our case. When considering a choice between Eu and Re, the latter is more frequently chosen as a similitude criteria [18,21], and is well suited because viscosity (through its influence on head losses) plays an important part in the present case. Thus, given the author's interest in the flow fields inside the CQ, we chose to base the similitude on the Reynolds number: $Re = u \cdot l / \nu$ for the flow structure, where u is the velocity [m/s], l the characteristic length [m] and ν the kinematic viscosity of the fluid [m²/s]. Due to the complex geometry of the reduced-scale model, the influence of head losses cannot be ignored and since head losses are influenced by the Reynolds number, reinforcing its choice as a similitude criterion. The head losses inside the CQ influence the duty points of the pump (for the 1:4 model) and of the fan (for the 1:1 model). To meet the Reynolds similitude criteria, the length, viscosity and velocity scales as well as the relationships between other derived flow parameters are presented in Table 1.

Table 1 Similitude criteria and model design dimension scales

| Similitude criteria: Reynolds number (Re) | | | | |
|-----------------------------------------------------------------------------------------------------------------|---------------------------|---------------|---------------------------|--------------|
| $Re_{water} = Re_{air} \Rightarrow u_{water} \cdot l_{water} / \nu_{water} = u_{air} \cdot l_{air} / \nu_{air}$ | | | | |
| Physical parameter scales during the design process | | | | |
| Type | Scale | Symbol | Relationship | Value |
| imposed | Length scale | S_L | l_{water} / l_{air} | 1/4 |
| | Viscosity scale (at 20°C) | S_ν | ν_{water} / ν_{air} | 1/15 |
| derived | Velocity scale (at 20°C) | S_u | u_{water} / u_{air} | 4/15 |
| | Surface scale | S_S | S_L^2 | 1/16 |
| | Flow rate scale | S_Q | $S_u \cdot S_S$ | 1/60 |

2.2. Using fan operating curves as boundary conditions in the numerical models

Experimental determination of the axial fan's actual operating curve

Airflow simulation of ventilated spaces generally uses measured velocity distributions as boundary conditions when very complex diffusers generate the ventilation jet [29]. If the geometry of the room or enclosure to be studied does not permit the measurement of a velocity profile at a diffuser's exit, an alternative is the simulation of the ventilation circuit itself. Although complex modelling of fan geometries in CFD simulations have been previously reported [30–33] with good results, these choices are costly in terms of computational power especially when coupled with complex ventilation circuits. Thus, our choice was for an equivalent method oriented towards the simulation of the axial fan based on its operating curve [34–38].

Any fan is characterized by its operating curve. The operating curve, given by the manufacturer is not always representative of the fan's actual behaviour. Consequently, we had to develop an experimental procedure allowing us to measure the axial fan's performance, which will be developed in the following chapter.

A steady-state simulation using a fan curve boundary condition will stabilise itself at a certain flow rate along the fan curve. This flow rate represents the intersection of the system curve and the fan curve at the imposed fan speed, defined in hydraulic installations as the duty point. Using the pump affinity laws ($Q_1/n_1 = Q_2/n_2$), knowing the flow rate determined by the CFD simulation (Q_1) and the measured fan speed imposed as a boundary condition (n_1), the fan speed (n_2) required for obtaining a desired flow rate (Q_2) can be calculated. When imposing this desired fan speed (n_2) as a boundary condition in the numerical model the resulting flow will be Q_2 .

The advantage of using the fan curve as a boundary condition over the habitually used measured velocity profiles is the ease of measurement. Determining a fan's operating curve does not require expensive lab equipment and is less subjected to problems of measurement resolution. It must be noted that for this method to work, the entire ventilation circuit upstream of the diffuser must be simulated as well leading to increased computational costs, which explains the simulation in two stages adopted here.

3. Material and methods

3.1. Design of the full-scale CQ experimental model and fan operating curve experimental measurements

Two axial fans (model EBM Pabst 4184 NXH) are used to ventilate the cabin, one for the intake of the air and the other for its exhaust (Figure 2a, b). This configuration was chosen for safety reasons, to avoid the risk of asphyxiation of the crew member, if one of the fans stopped during his/her sleep. The fans are powered via a 24V direct current connection, with the previously mentioned three-step speed control configuration (low, medium, high) [6].

The ducting system is lined internally with soundproofing material. The geometry of the air introduction circuit is quite intricate (Figure 3 a, b) with two elbows (of 90° and respectively 180°) and a system of guiding vanes. All these components have a primary role in the dissipation of the noise coming through the ducting from the ISS corridor (background noise) and from the axial fans themselves [6,8].

The intake fan is placed inside a plenum at the beginning of this ducting system (Figure 3 b). The air extraction circuit from the cabin has a shorter circuit and does not present particular characteristics. The second axial fan is placed inside a plenum as well, at the beginning of the exhaust ducting (Figure 3 b).

The interior surface of the CQ is covered with several layers of soundproofing materials (a Kevlar® wool pad with white Gore-Tex®, and Nomex® assembled in a quilted structure) that serve to mitigate the propagation of acoustic waves through the walls of the cabin structure [8].

In our laboratory we developed a full-scale mock-up of the CQ (Figure 2). The dimensions of the CQ and its ventilation system were extracted from its design documents [5,6,8], and the dimensions of the standard racks on the ISS [17]. The racks are modular units, which can be detached from the ISS and replaced, generally housing vital systems and/or laboratory equipment. The crew quarters were designed to fit within such a rack since, they were designed after the conception of the ISS and as such did not have a previously designated space.

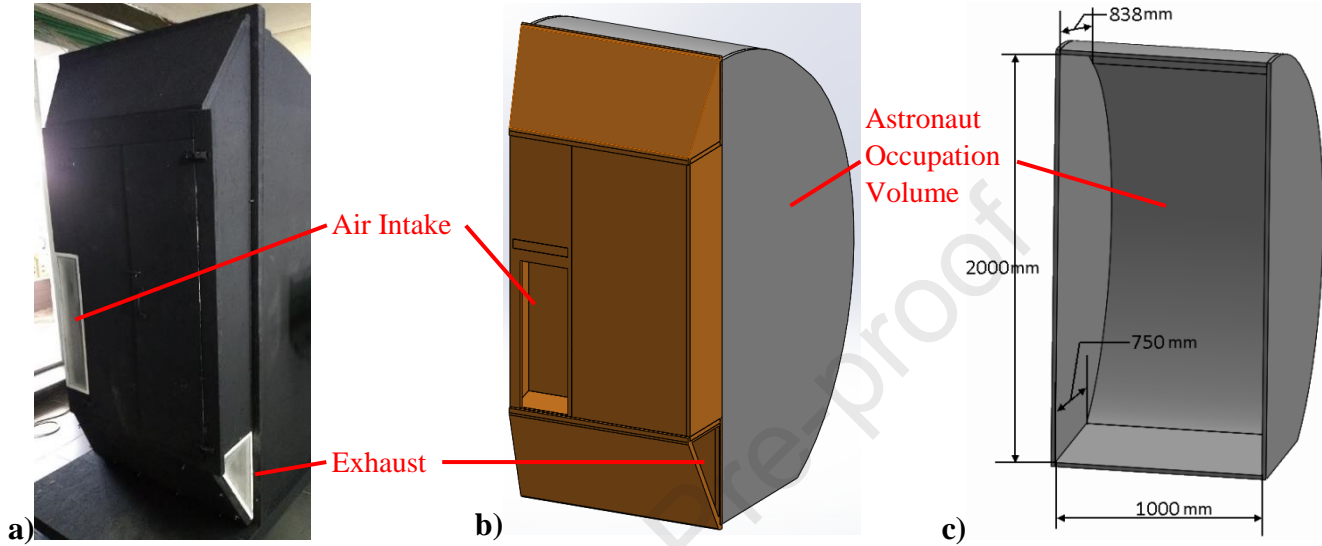


Figure 2 Full-scale CQ mock-up (a), 3D representation of the mock-up with the bump-out (containing the ventilation ducts and the door) highlighted (b), mock-up interior (c).

The replica of the CQ was built from Oriented Strand Boards (OSB) fixed together with screws. The air diffuser was manufactured to reproduce the one in the ISS CQ. Several cut-outs were made near the ventilation circuits to enable access inside and allow modifications and or intervention in case of emergency. As can be seen in Figure 3 c, when the ventilation duct mask is removed, the fan inside can be seen encased in polystyrene to diminish vibrations transmitted to the structure, similar to the fan on the ISS CQ. The interior of the CQ mock-up was covered with the same soundproofing materials as the ones used on the ISS CQ. This 1:1 scale mock-up of the CQ allowed us to perform several experimental studies such as the one presented in [25] describing the CO₂ accumulation tendency curves, that served for the validation of a numerical model reproducing the transient human breathing and the evolution of the CO₂ concentration inside the CQ without ventilation. Other measurements were possible in the CQ replica, which are not given in this paper, dealing with the analysis of noise propagation in order to reduce the acoustic signature of the fan in the CQ.

Even if this full-scale mock-up was not used for the validation of the numerical model in this study, it allowed us to master all the geometric and technical details required to develop the reduced scale mock-up.

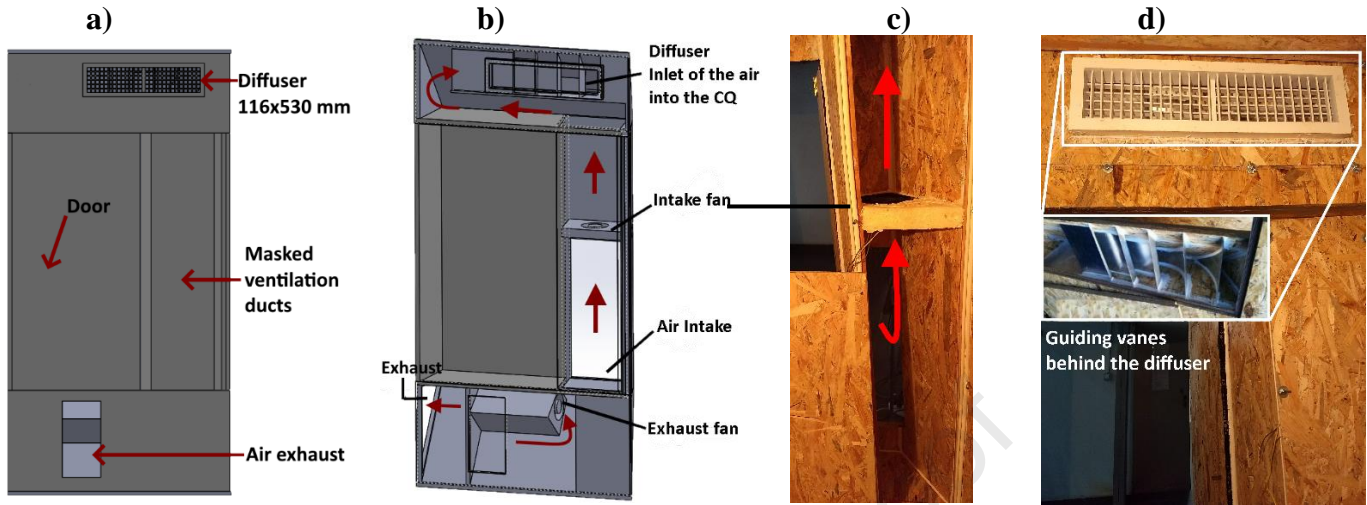


Figure 3 Interior view of the bump-out (a) with the ventilation circuit and fan placement (b); Interior view of the ventilation ducts and the intake fan placement (c) along with the ventilation diffuser and its guiding vanes (d).

As previously mentioned, the following step is the experimental measurement of the AF's operating curve. An experimental set-up (Figure 4) was built in the present study to determine the real fan curve used in the 1:1 mock-up (the same fan as the one used in the CQ aboard the ISS, Figure 4), which will be introduced in the numerical model.

The experimental set-up for measuring the fan operating curves was designed as a wooden cubic box with a hollow interior, with the side length equal to five times the diameter of the fan. This ratio has been chosen to allow a good development of the flow inside the box. The fan was centrally mounted on one side of this box and the circular evacuation outlet (with a diameter equal to that of the fan) was built on a perpendicular side. The perpendicular outlet introduces additional head losses in the system as opposed to a location on the opposite wall of the axial fan, and allows us to better measure pressure differences. This set-up was not chosen arbitrarily, a similar one was used by NASA during the design of the CQ for the characterization of the same axial fans [12]. The flow rate was varied by means of circular orifice plates of various known diameters - D_{exhaust} , varying in 1 cm increments between a diameter of 11 cm, approximately equal to that of the fan, and 0 cm which means a closed flat plate corresponding to the null flow state. On each plate there is a graded ruler in increments of 0.5 cm which allows the positioning of an anemometer along the radius of the circle, the ultimate goal being to integrate the velocity profile measured on the known surface of the orifice in order to obtain the flow rate. With the velocity profile determined for a known surface, the points being drawn at known distances, the flow rate can be determined by integrating the velocity over the surface by the trapezoidal rule.

Since the fan curve is described by the variation of the pressure head as a function of the volumetric flow rate, these parameters needed to be measured on the experimental setup described above. The fan flow rate variation is obtained by introducing head losses at the box outlet without changing the fan operating parameters, by using the circular orifice plates. The pressure differences between the interior of the box and the outdoor environment at atmospheric pressure were measured offering the pressure head component of the curve. Velocity profile measurements, vertically and horizontally across the box outlet (Figure 4, Figure 5a) allow flow rate estimation across the orifice. From the pairing of each volumetric flow rate with its associated pressure head, the fan operating curve is constructed (Figure 5b).

The axial component of the velocity was measured with a hotwire probe thermo-anemometer (Kimo VT110) – measuring from 0.15 to 30 m/s with an accuracy of $\pm 3\%$ reading, ± 0.05 m/s in the 0.15 to 3 m/s range and respectively of $\pm 3\%$ reading, ± 0.2 m/s in the 3.1 to 30 m/s range. The hot wire anemometer was fastened at the appropriate height via a tripod and two average velocity values were recorded over 1 minute for each point along the

radius. Two measurements were made for each point to establish the repeatability of the measurement procedure. The pressure difference was measured with a differential micromanometer KIMO MP110 having the accuracy of ± 2 Pa. The measured pressure difference was also obtained as an average of pressure fluctuations for 1 minute.

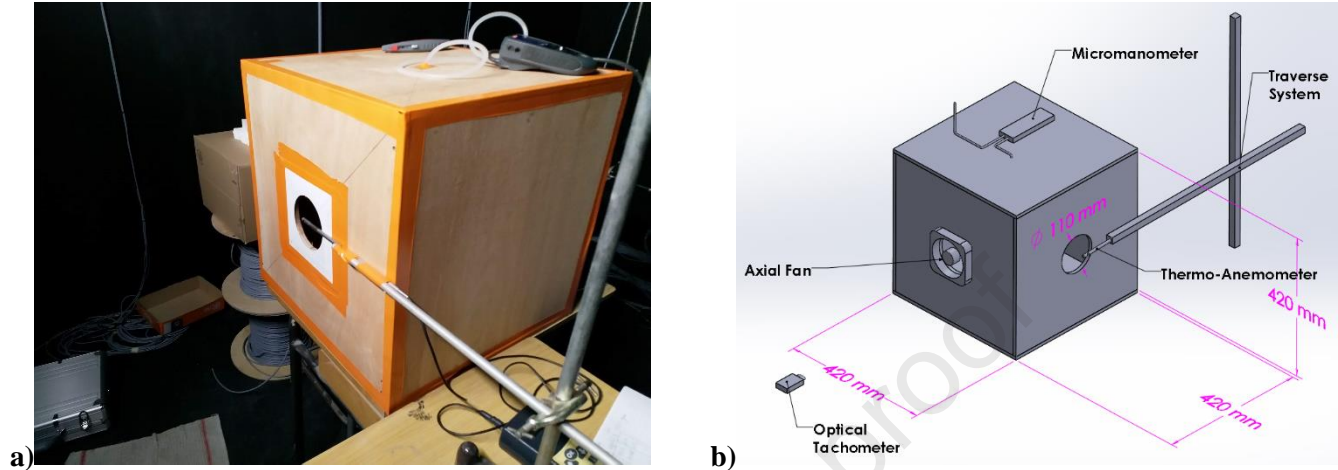


Figure 4 Experimental setup used to measure the axial fan head-flow curves: photo (a) and schematic (b) showing the positioning of the fan and the tachometer, the manometer, exhaust opening and anemometer positions.

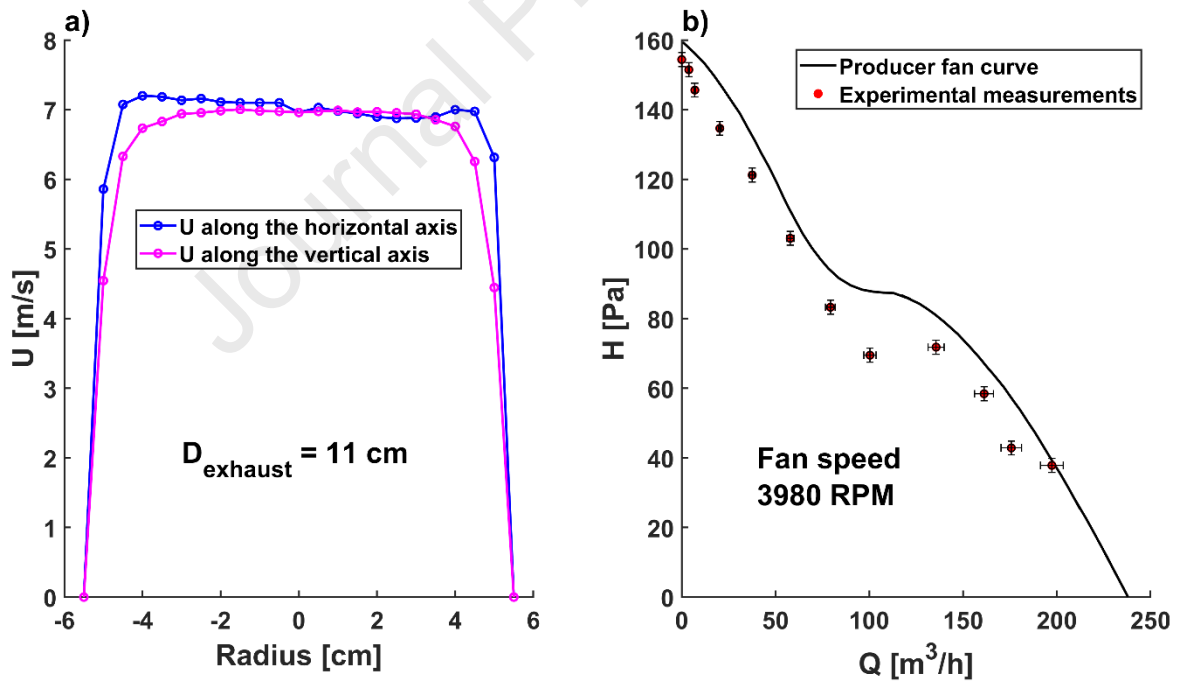


Figure 5 U velocity profiles along the horizontal and vertical axes at the adjustable exhaust for a $D_{\text{exhaust}} = 11$ cm (a), the producer fan curve compared to the experimental measurements (b).

The fan has been powered by a direct current source at its rated voltage of 24 V. The actual fan rotation speed is important in order to determine the flow through the ducting system in our case. This was measured with an optical tachometer oriented towards a reflective strip placed on one of the fan blades.

Figure 5a shows two axial velocity profiles (vertical and horizontal) measured at the exit plane of the orifice of $D_{\text{exhaust}} = 11$ cm. This is the maximum difference between two measured profiles since at lower diameters, the horizontal

and vertical profiles collapse allowing us to consider that the flow is symmetric. This subsequently allows the integration of the axial velocity along a radial direction to determine the flow rates for each value of D_{exhaust} .

Figure 5b presents both the head-flow rate experimental curve that was determined as previously explained and the curve provided by the manufacturer. It can be seen that the experimentally determined pressure head display slightly smaller values than the one provided by the manufacturer. In the following part of the study the experimental operating curve will be correlated with the measured fan speeds to provide a boundary condition for the numerical model. Knowing the pressure drop in the actual ventilation circuit, the duty point can be determined at a known speed, and then through the pump affinity laws, the speed required to obtain the flows used by NASA (108, 138 and 156 m^3/h) can be determined [6].

3.2. Design of the reduced-scale CQ experimental model for PIV measurements

The small-scale model following the length scale $S_L=1/4$ (Table 1) was manufactured out of transparent acrylic (Figure 6b) of optical quality to allow velocity measurements using the PIV technique. The model was supplied with water in a closed loop using a pump to ensure the control of the flow rate. The hydraulic circuits upstream of the diffuser grille and the extraction were reproduced as close as possible to the full-scale mock-up (distributing the flow upstream the diffuser grille with the same guiding vanes and bends). Previous attempts to design a simplified inlet and outlet circuits resulted in a distorted flow field downstream of the inlet diffuser. To this end, a flow distributor was constructed as can be seen in Figure 6b. It was equipped with precise control valves enabling the control over the flow rate through each tube of the distributor supplying each channel with water flow. The reduced scale model is equipped with a removable lid, enabling us to place a human model inside that was obtained through additive manufacturing (3D printing). This human model is an S_L scaled version of the human model used in the numerical study (a human of height 1.8 m, resting in the neutral position of the body in microgravity [1]) and it was placed at the same height as the test subjects were seated during the experiments in our previous study [25]. The blueprints for the human body used in the numerical model were chosen to fit the scale and to keep the proportions of one thermal manikin that was developed in our team [39,40].

The diffuser grille was also designed as a $1/4^{\text{th}}$ scale replica of the one placed in the full-scale mock-up. However, it was slightly modified when manufactured. due to the diffuser guiding fins, which, when scaled to $1/4^{\text{th}}$ of their size would have to be 0.5 mm thick, compromising their structural integrity. An imperfect reproduction of the diffuser grille led to a slight alteration in its associated length scales which have been taken into account further in this study and presented in Table 2.

Table 2 Dimension scales of the diffuser grille post-manufacturing process

| Scale | Symbol | Relationship | Value |
|-----------------|------------------|-------------------------|--------|
| Length scale | $S_{L-diffuser}$ | l_{water}/l_{air} | 1/4.1 |
| Viscosity scale | S_v | ν_{water}/ν_{air} | 1/15 |
| Velocity scale | $S_{u-diffuser}$ | u_{water}/u_{air} | 4.1/15 |
| Surface scale | $S_{S-diffuser}$ | S_L^2 | 1/16.8 |
| Flow rate scale | $S_{Q-diffuser}$ | $S_u \cdot S_S$ | 1/63 |

Other elements present on the reduced scale model are an automatic air purge valve situated on the top of the model close to an edge, so as to not influence the PIV measurements, and reinforcement elements on the outside of the small-scale model for better mechanical resistance.

In this study, we have employed a Dantec Particle Image Velocimetry (PIV) system for the velocity field measurements. This system is composed of one high sensitivity Flow Sense EO camera of 4×10^6 pixels resolution and of a Dual Power 200 mJ laser having the wavelength of 532 nm. The acquisition frequency of the PIV system was 5 Hz. The water flow was seeded with fluorescent polymeric spheres with a mean diameter of 20 μm . The image calibration gave a spatial resolution of 280 μm per pixel, which corresponds to a $560 \times 560 \text{ mm}^2$ field of view. The PIV measurements were performed in 5 different planes whose positions and orientations are presented in Section 2.

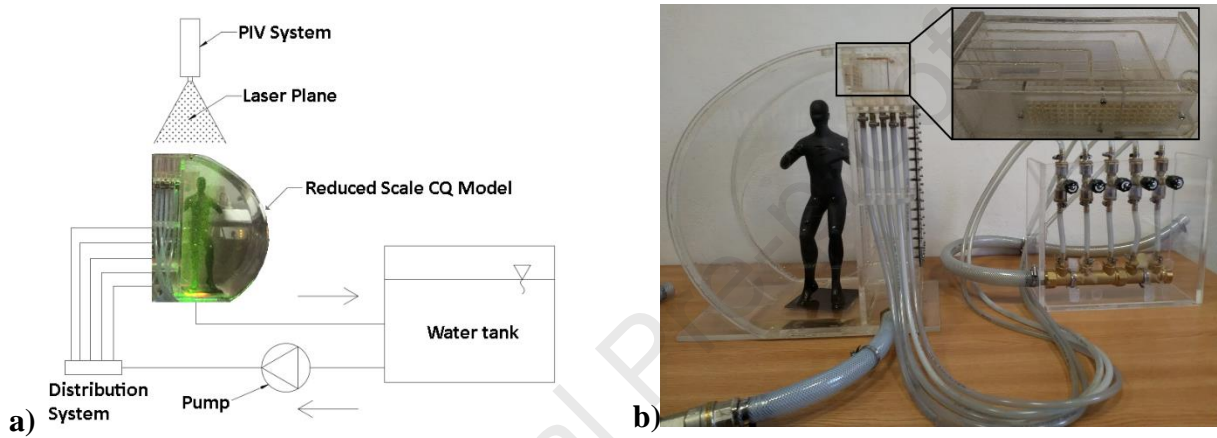


Figure 6 Schematic representation of the PIV measurement setup (a) and the reduced scale mock-up along with its water distribution system (b).

The parameter monitored in the PIV study was the flow rate through the installation. A portable ultrasonic flowmeter (GE PT900) with an accuracy of $\pm 1\%$ of reading was installed on a straight section of the pipe between the pump and the distribution system, 10 pipe diameters away from any element that could introduce minor head losses (bends, valves etc). The flow was measured with a frequency of 1 Hz for 30 minutes prior to the start of the PIV measurements resulting in a stable flow rate $Q_{water} = 35.5 \text{ l/min} = 2.13 \text{ m}^3/\text{h}$. This flow rate corresponds to $Q_{air} = 2.13 \cdot 63 = 134.2 \text{ m}^3/\text{h}$ (Table 2) a value close to the median flow rate on the ISS CQ ($138 \text{ m}^3/\text{h}$ [8]) and will be used as a calibrating parameter for the numerical model following the length scales presented in Table 2.

3.3. Numerical model design and choice of the boundary conditions

The role of the numerical model developed in this study was to reproduce the existing solution of the general ventilation system of the CQ aboard the ISS, in order to offer a detailed picture of the flow patterns inside the cabin. The validated model will then be useful to find different solutions of airflow optimization in order to avoid the presence of CO_2 accumulation pockets in the breathing zone of the astronaut inside the CQ. To this end, we developed a numerical model allowing a faithful reproduction of the flow through the ducts, through the diffuser and the exhaust grille. One of the main difficulties was to find the best compromise between the reproduction of the complex flow introduced by the axial fan into the air distribution system and the available computational resources.

Two numerical models were developed over the course of this study; the first one was used in order to reproduce the complex flow generated by the axial fans through the ducting system and through the diffuser, and the second for achieving the primary goal of our investigation, namely, the modelling of the air distribution inside the CQ in the presence of a human model representing an astronaut. As mentioned before, our choice was related to the best

compromise in terms of accuracy and computational resources, this way, we decoupled two problems. In a first step the fan curves were used as boundary conditions and the airflow through the ducts, the guiding vanes and through the diffuser were solved together with the air distribution in a CQ model without the presence of the human model. In a second step, we imposed the velocity distribution obtained at the exit of the diffuser from the first model to the inlet of the second model with the body of the astronaut inside.

The numerical results from the second model were compared with the detailed PIV measurements performed in the reduced scale CQ mock-up.

The first numerical model (denoted Model 1) is a faithful reproduction of the full-scale CQ mock-up including the previously presented ducting system (Figure 3) and the fan emplacements. It has a tetrahedral mesh of 5.5 million cells and 6 cells in the boundary layer near the walls. The mesh detail, cell count and sizes are presented in Figure 7a. Denser mesh regions are found around the intake and exhaust fans and at the ventilation diffuser grille. Each diffuser orifice (a square of 2 cm length) has around 40 cells across each side. Following a mesh independence study augmenting the mesh size to over 6 million cells lead to diminishing returns in convergence criteria and result accuracy, when taking into account the computational requirements. Tetrahedral cells were used here given that polyhedral cell tests performed poorly because of the cell quality around the guiding vanes that are found upstream of the diffuser grille.

For this first numerical model, the fans were represented as two distinct fluid regions, shaped as a hollow cylinder whose thickness corresponds to the fan blade length and whose hollow centre corresponds to the fan rotor. On the upstream face of these hollow cylinders the fan boundary condition was imposed by defining the measured fan curve in the CFD software and specifying the fan speed.

The experimentally measured fan curve can be used to control the flow rate inside the numerical model. Table 3 presents the initial flow rate for the measured fan speed, along with the fan speed necessary to obtain the equivalent flow rate of the experimental PIV measurement using the reduced scale model.

Table 3 Flow rate and fan speed correlation for Numerical Model 1

| | Fan speed (boundary condition) | Flow rate (computed) |
|---------------------------------------------------------------------|--------------------------------|-----------------------------------------|
| Experimentally measured fan speed | $n_1 = 3980 \text{ [rot/min]}$ | $Q_{air1} = 114 \text{ [m}^3\text{/h]}$ |
| Required fan speed for the equivalence with the reduced scale model | $n_2 = 4680 \text{ [rot/min]}$ | $Q_{air2} = 134 \text{ [m}^3\text{/h]}$ |

Numerical model 1 was used to calibrate the fan curve boundary condition and ultimately obtain a flow rate of $134 \text{ m}^3\text{/h}$ throughout the ventilation circuit - the equivalent flow rate of the $2.13 \text{ m}^3\text{/h}$ measured during the PIV tests. This value accounts for the scale alterations of the diffuser grille presented in Table 2, as the flow scale is $S_{Q-diffuser} = Q_{air2}/Q_{water} = 62.9$ presenting an error of 0.15 % from the theoretical value (Table 2). A velocity profile was extracted inside the CQ at the grille exit, presented in Figure 8 and the general flow pattern matches that reported for the CQ on the ISS [8]. This profile was extracted from numerical model 1 (Figure 7a) and introduced in numerical model 2 (Figure 7b) as a boundary condition on the diffuser.

The second model (Figure 7b) contains only the inside volume of the CQ along with the human model situated where the astronauts normally sleep. The human model takes the neutral position of the human body in microgravity, and it corresponds to the small physical model manufactured through additive techniques (Figure 6b). The second numerical model has a mesh composed of 3.5 million polyhedral cells with 5 cells in the boundary layer near the walls of the CQ and the surface of the virtual astronaut. Denser mesh areas are found around the diffuser and the walls of the model as shown in Figure 7b. Similar to the first model, after a mesh independence study, the second mesh proved to offer a good balance between accuracy and computational requirements. This time, polyhedral cells provided superior

convergence parameters during the testing.

The boundary conditions and design criteria for the two numerical models are presented in Table 4.

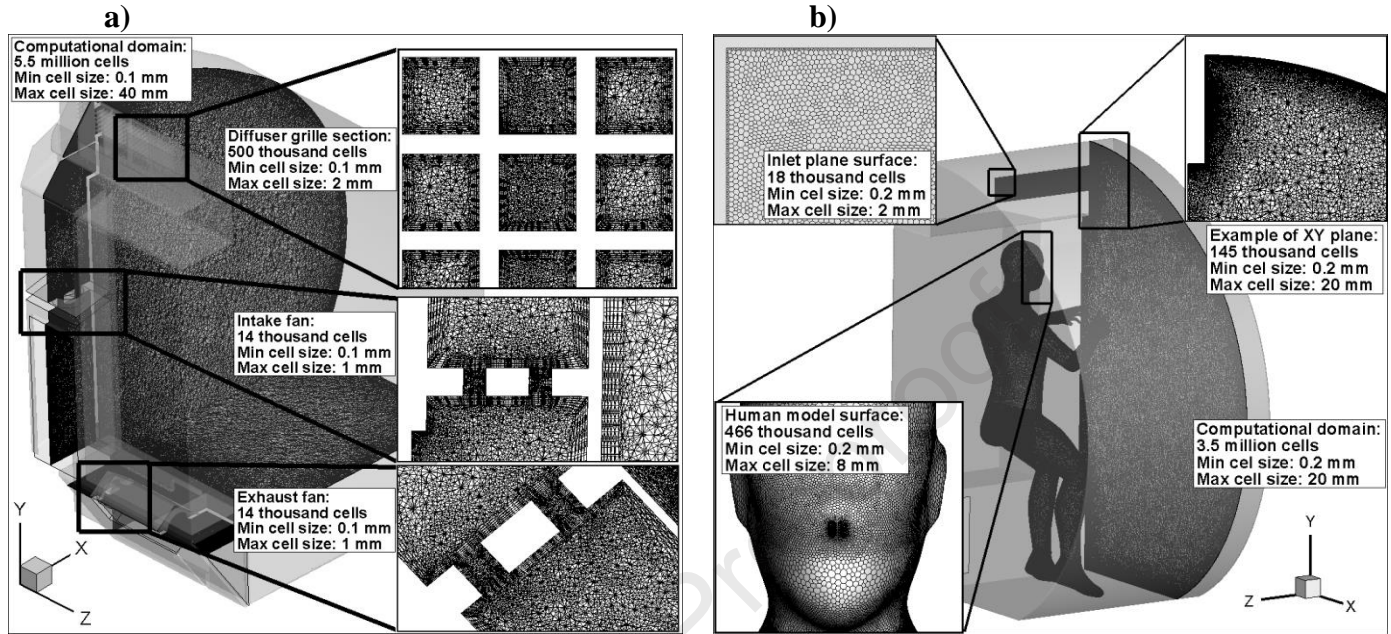


Figure 7 Mesh cell number and size details of the two numerical models; Model 1, the one used for determining the diffuser velocity distribution (a) and Model 2 used for cabin flow study validated with PIV measurements (b).

Table 4 Numerical parameters and boundary conditions for the two numerical models

| | Numerical Model 1 (Figure 7a) | Numerical Model 2 (Figure 7b) |
|---------------------------------|--------------------------------------------------------------------|-----------------------------------------------------|
| Diffuser grille Reynolds number | ~14,000 | ~14,000 |
| Turbulence model | Realizable k- ϵ Enhanced Wall Functions | Realizable k- ϵ Enhanced Wall Functions |
| Inlet boundary condition | Pressure inlet (0 gauge pressure) | Velocity Inlet User-defined Velocity Profile |
| Outlet boundary condition | Pressure Outlet (0 gauge pressure) | Pressure Outlet (0 gauge pressure) |
| Fan boundary condition | Experimentally Measured Fan Curve | N/A |
| Pressure-velocity algorithm | Coupled | Coupled |
| Spatial discretization scheme | Second Order Upwind | Second Order Upwind |
| Convergence criteria | Stable Flow Rate + (Parameter Stability or Residuals < 10^{-6}) | Parameter Stability or Residuals < 10^{-6} |

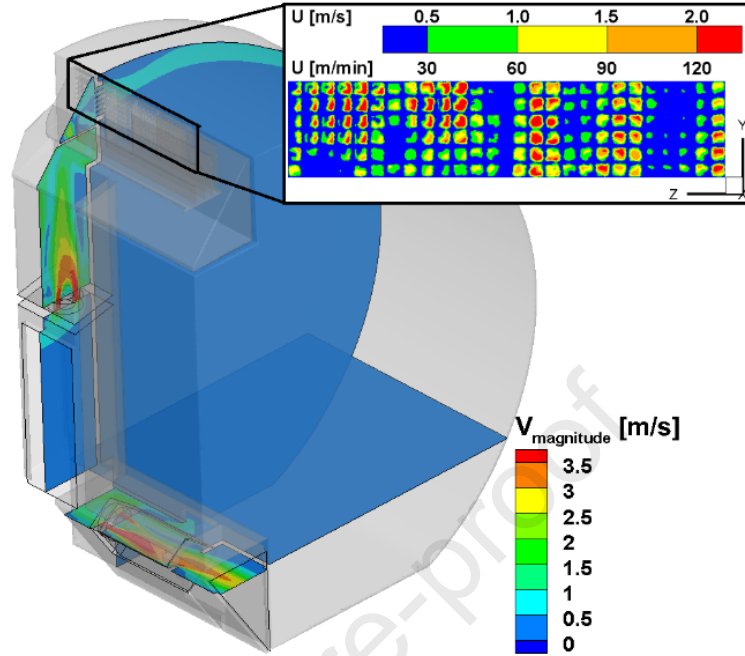


Figure 8 Axial fan median planes for numerical model 1, used to determine the diffuser grille velocity distribution (in m/s and m/min for comparison with study [8]).

Figure 8 presents the velocity magnitude distributions in the axial fan's median planes for numerical model 1, used to determine the velocity distribution at the diffuser grille that is also visible in this figure. This distribution was compared with the one obtained during the onboard evaluation of the air diffusion system in the CQ on the ISS (presented in [8]). We note here that there is a certain difference in resolution between the experimental measurements performed on the ISS and our numerical results. It is specified in the literature [8] that the measurements were made in the centre of each orifice of the ventilation diffuser, but the measuring instrument used was not specified (it results from the text of [8] that a thermo-anemometer might have been employed). In [8] it could be observed that for each elementary orifice composing the diffuser two or more velocity values are divided by a diagonal line, suggesting that an interpolation has been made following the measurements. The nature of this interpolation is not described, therefore the differences in resolution between the two images should be considered in the comparison. Other differences between the two results (the one presented in Figure 8 and the one from [8]) are due to several factors. Firstly, the 1:1 scale follows the CQ design on the ISS as close as possible, but there is a difference due to the lack of exact design plans. Elements such as the construction of airways, their radius of curvature, their exact size can be estimated with good accuracy, but even slightly small upstream differences can change the downstream flow behaviour. All these elements influence flow parameters, but the overall air distribution trend is similar in the grid upstream circuit between the 1:1 CQ scale mock-up and the ISS measurements.

4. Results and discussion

Figure 9a presents the locations - respectively the planes noted with P1, P2, P3, P4, P5 - where the PIV measurements were performed on the reduced scale model. In Figure 9 and in all subsequent figures, the dimensions of the X_N , Y_N and Z_N axes are normalized by their maximum lengths in the corresponding model to allow comparison between the numerical 1:1 scale model and the experimental 1:4 scale model.

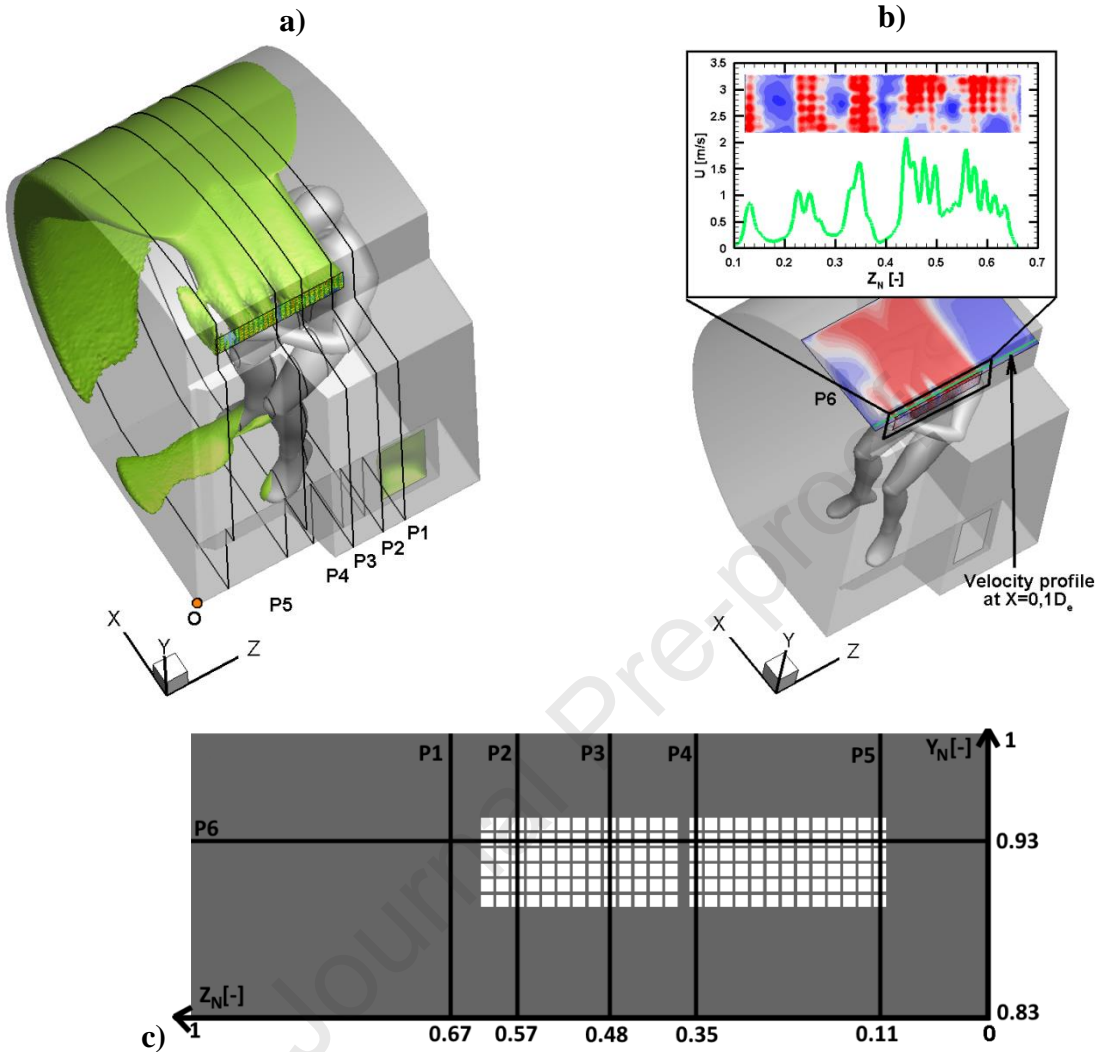


Figure 9 Exterior view of the numerical CQ model with velocity iso-surfaces at a value of 0.5 m/s, and the highlighted position of the five vertical planes (P1-P5) (a); streamwise velocity profile at $X=0.1D_e$ in front of the diffuser in plane P6 (b); interior view of the ventilation diffuser showing the six planes (P1-P6) (c).

In planes P1-P5, we also extracted the distribution of the velocity components from the second numerical model. The reader might visualize the disposal of these planes in relation with the flow inside the cabin through the velocity iso-surfaces of 0.5 m/s. A 6th plane (P6) is also represented in Figure 9b, in which we do not have experimental data, but which represents a horizontal observation plane ($Y_N=0.93$, see Figure 9c) corresponding to the peak of the velocity profiles of the curved wall jet (Figure 10). P6 allows us to observe a transverse evolution of the flow issuing from the diffuser in its near region that is partially subjected to a Coanda effect [41] (Figure 9b) leading to a horizontal incurvation of the flow trajectory toward the vertical lateral wall of the CQ. Also, one can observe in the top of Figure 9b, that the flow near the exit of the diffuser, close to the diffuser is characterized by a complex interaction between each small jet generated by each grid element of the diffuser. Larger flows regrouping bunches of these elementary jets are formed due to the combined effect of the axial fan, the air circuit, the disposal of the guiding vanes behind the diffuser, as well as the cross-interaction of elementary jets. These larger flows evolve at around $X_N=0.12$ into one single general jet that soon attaches to the curved wall of the CQ. From the observation plane P6 (Figure 9b) the streamwise initial velocity profile has been extracted at a distance $X_N=0.016$ ($X=0.1D_e$) from the diffuser, giving a local view of the complexity of the flow at the exit of the diffuser.

The overall flow patterns and differences in flow behaviour from a plane to another (P1 to P5) are well captured by numerical model 2. The absence of flow in the initial region of the CQ roof ($X_N < 0.1$) on P1 is explained by the position of P1 outside the grid (Figure 9c). The related jet expansion in Z_N -direction confirms the three-dimensional behaviour of the jet flow in the cabin. The Coanda effect is clearly visible only on P5, particularly in the numerical case. For the others planes, it is difficult to say which is the preponderant phenomenon (Coanda or impinging); the recirculation region formed between the upper frontier of the jet and the curved wall is a region of low pressure, resulting from confinement and subsequent jet entrainment deficit. Figure 10 displays a zoom-close to the jet exit in plane P4. In this figure, the in-plane velocity vectors were superposed on the contours of the velocity magnitude. The velocity magnitude in the PIV measurements (V_m^* [m/s]) was divided by its factor of similitude ($S_u = 4/15$) to obtain the values that would appear in the full-scale model and was represented with the same notation as the velocity magnitude in the full-scale numerical model (V_m [m/s]). The recirculation region is fairly well reproduced, both qualitatively and quantitatively by the numerical model, with one small difference: the attachment region, which occurs in both cases between $X_N=0.25$ and $X_N=0.40$, is steeper in the numerical case compared to the experimental case. Knowing the difficulties in measuring and simulating a flow very close to a wall, it is difficult to judge here in which case the flow is the most realistic.

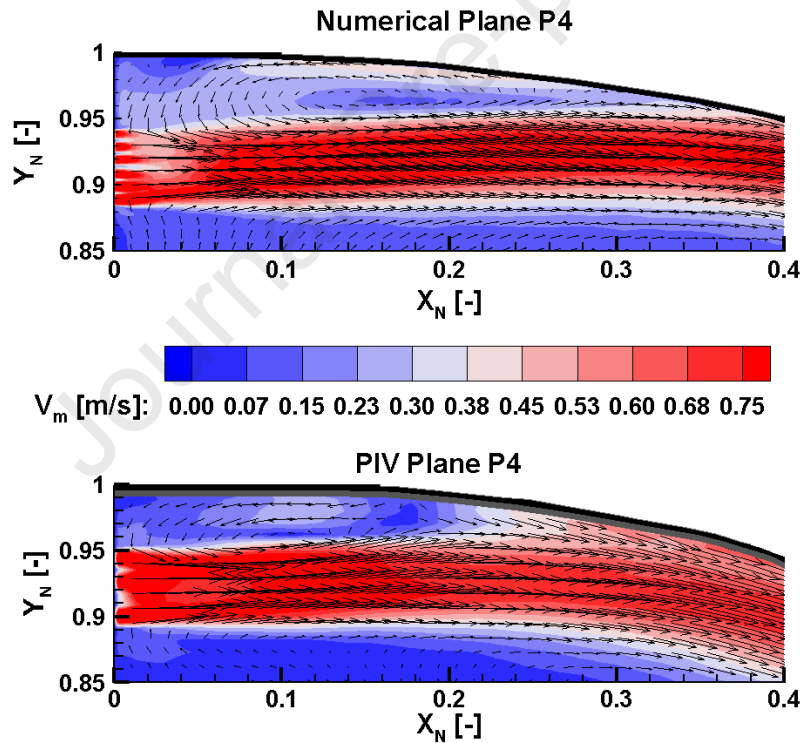
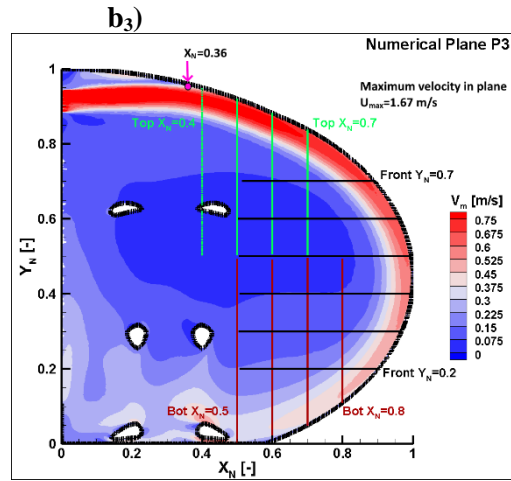
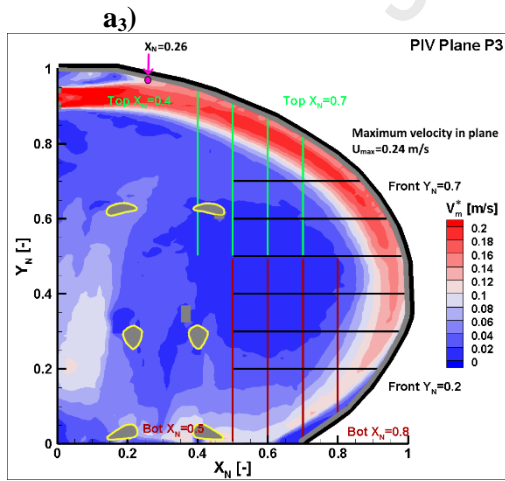
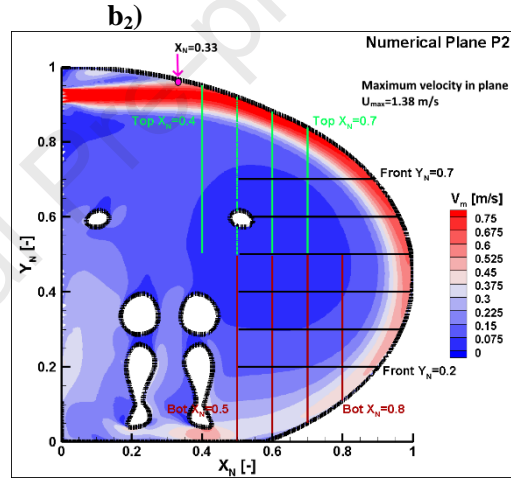
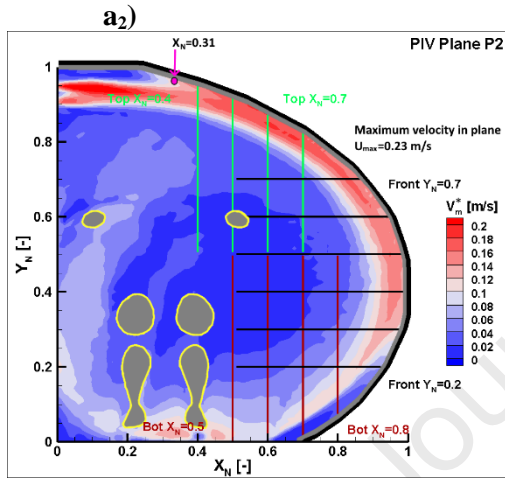
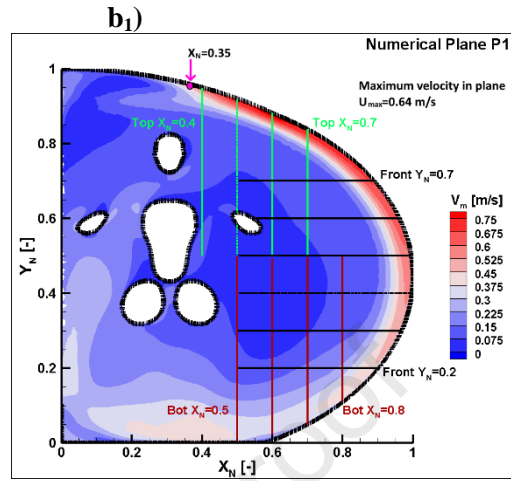
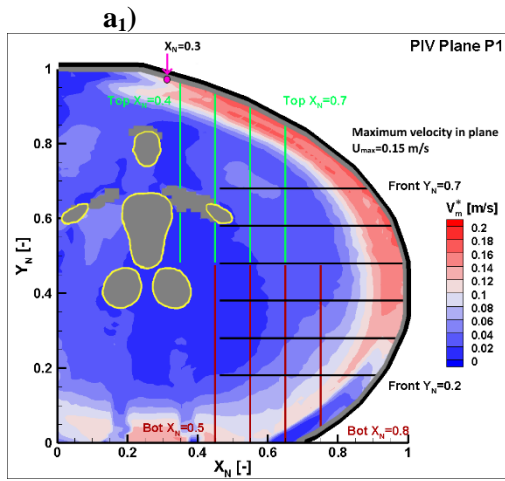


Figure 10 Zoom in the near exit region of the flow in plane P4 displaying a recirculation region.

For a more detailed comparison of numerical and experimental data, allowing the identification of the overall flow dynamics and the capability of the numerical model to capture it, we extracted several vertical and horizontal normalized velocity magnitude (V_{mN}) profiles in planes P1-P5 which can be seen in Figure 11 along with the points (purple colour) marking the beginning of the wall jet region.

In Figure 12 these profiles were superposed and compared. The colour coding corresponds to the one of the vertical and horizontal planes depicted in Figure 11 for P1-P5 and represent the numerical data while the black circles correspond to the experimental PIV data. The profiles in Figure 12 are presented in order following the trajectory of the ventilation jet along the curved wall (the first green profile corresponds to the first top profile at $X_N=0.4$ and the

last red profile corresponds to last bottom profile at $X_N=0.5$).



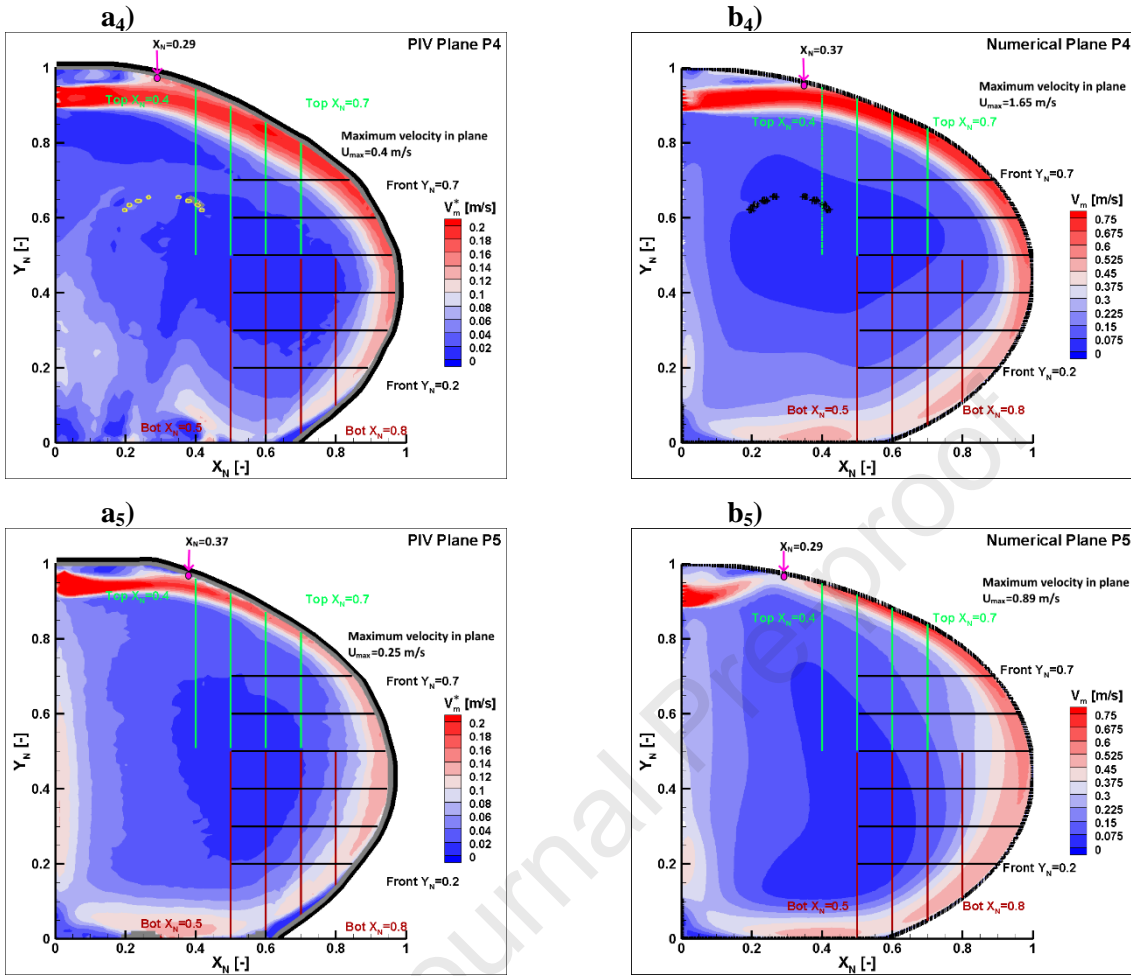
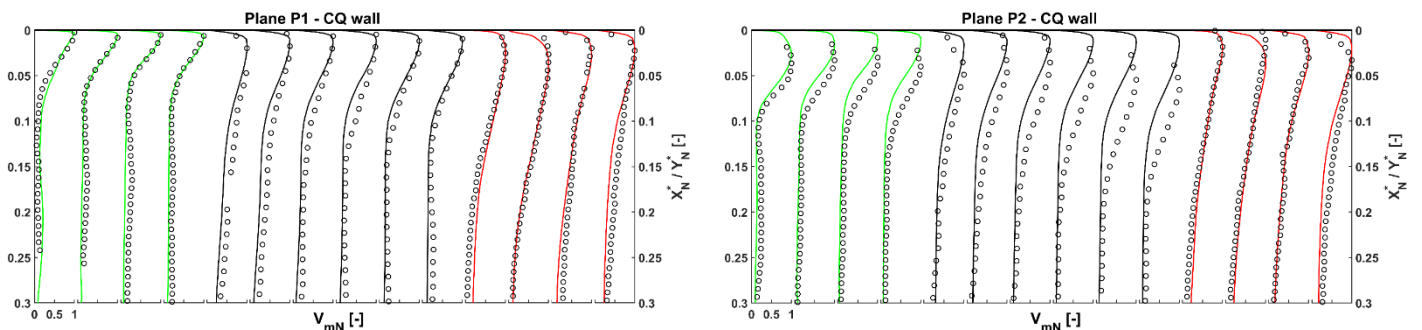


Figure 11 Comparison of experimental water flow fields (a_1 - a_5 left) and numerical air flow fields (b_1 - b_5 right) in planes P1-P5; cutting lines correspond to the velocity profile extraction reported in Figure 12.

One can see that in Figure 12 the overall pattern of the flow is similar between the experimental and numerical data, with the slight differences noticed before. Planes P1 and P5 are the most satisfactory among the observed planes the profiles being in good agreement between PIV and CFD results. Globally the flow pattern between the full-scale numerical results and the reduced scale experimental results inside the CQ is in accord. At this stage one can conclude that the numerical model validation is satisfactory, which give confidence in future studies using this model for improving the ventilation system of the CQ.



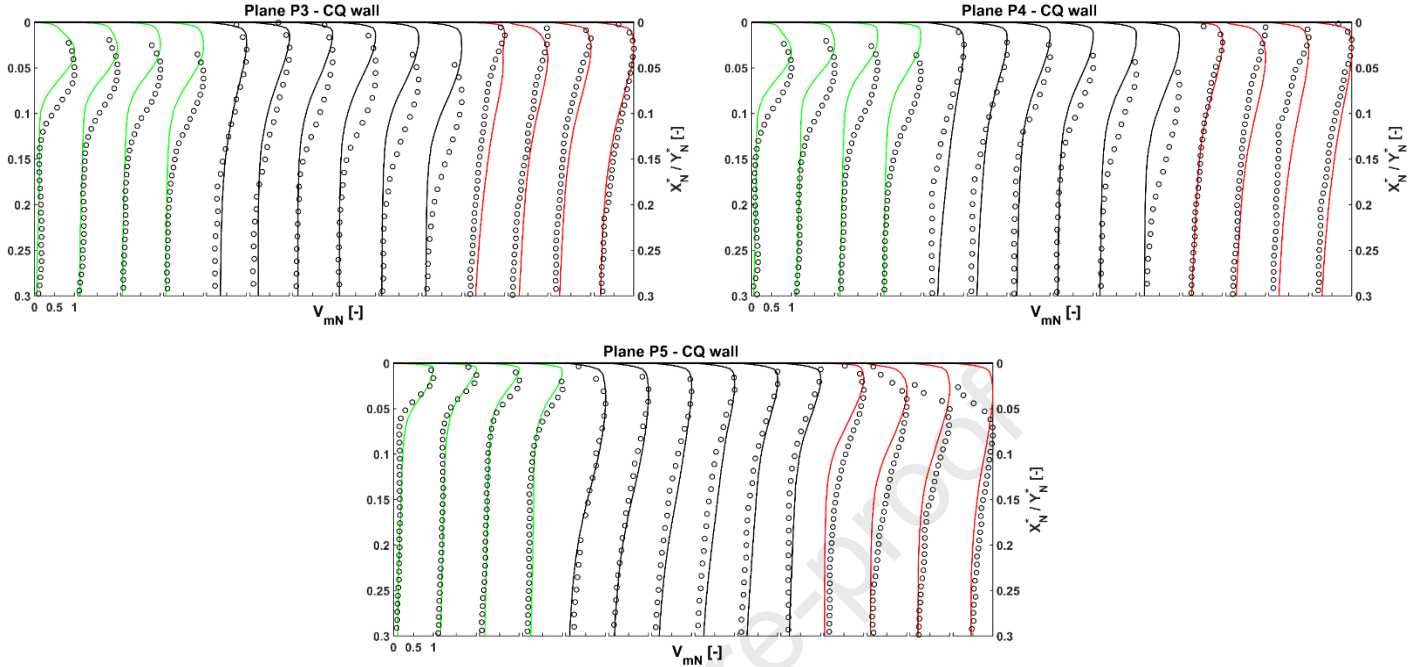


Figure 12 Normalized velocity profiles along the curved wall of the CQ in planes P1-P5, following X_N and Y_N according to the position of the profiles (Top, Front or Bot in Figure 11) – numerical data (solid lines) and experimental PIV data (black circles).

The ventilation system of the CQ aboard the ISS can be set to function at three different flow rates (108, 138 and 156 m³/h). The flow rate used in this study (134 m³/h) is close to the medium setting of the fan in the CQ (138 m³/h) to the extent that the flow fields can be considered similar. For the other two flow rate settings, the fan parameters were adjusted in the CFD model to enable a comparison between these cases and the simulation using 134 m³/h backed by experimental PIV results. The purpose of this comparison is to ascertain the influence of different flow rates (108, 138 and 156 m³/h), and consequently different Reynolds numbers (11000, 14000 and 16000 respectively), on the flow field inside the CQ.

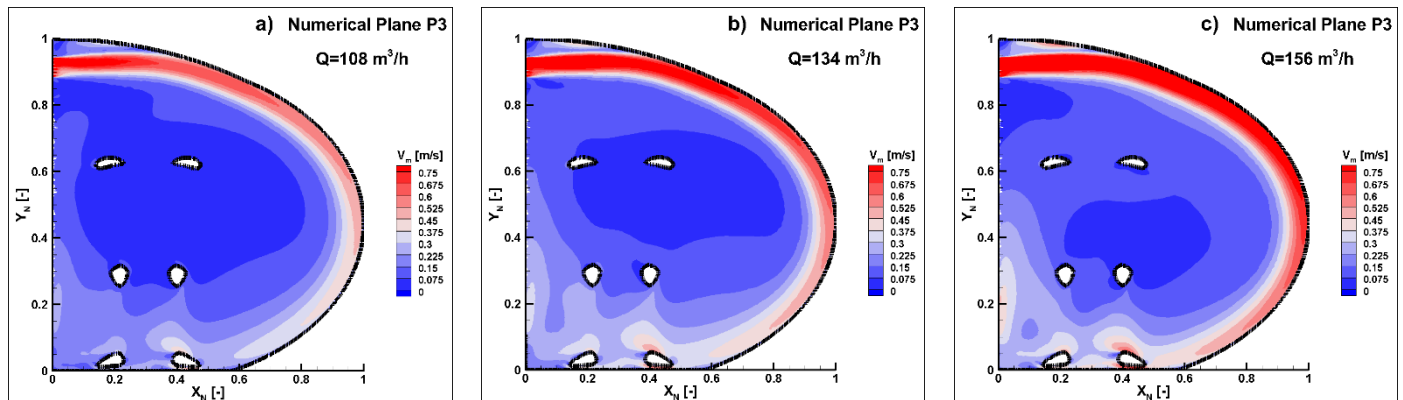


Figure 13 CFD comparison of the three different flow rates: 108 m³/h (a), 134 m³/h (b), 156 m³/h (c) in numerical plane P3, highlighting the effect of different Reynolds Numbers on the flow field.

The results presented in Figure 13 show a comparison of CFD Model 2 for the three flow rates previously mentioned. The conclusion of this comparison is that the flow field is not significantly altered. In all cases the ventilation jet attaches itself to the curved wall and causes the appearance of a stagnant air zone in the central area of the CQ where the human rests. This stagnation zone is slightly diminished when the flow increases, but even for the

highest flow rate ($156 \text{ m}^3/\text{h}$) velocity values in this area stay below 0.2 m/s . However, we recall that ISS reports [8,9] state that the $156 \text{ m}^3/\text{h}$ is less utilized by the occupants due to noise complaints. We can thus consider that the conclusions drawn from the CFD simulation at a flow rate of $134 \text{ m}^3/\text{h}$, validated by experimental PIV measurements in a reduced scale model in water, are generally applicable to the other two flow rates as well.

The air movements in the cabin generated by the general ventilation system (Figure 11), should ideally dilute the CO_2 that accumulates in the astronaut's breathing zone. Figure 14a presents the CO_2 concentration in plane P4, without gravity and without general ventilation, highlighting a region with high CO_2 concentration caused by the astronaut's breath determined in the authors previous work [25]. Figure 14b shows, in the same plane as Figure 14a, the velocity magnitude distribution in the ventilated CQ from the present study and serves to highlight the area that needs to be ventilated in order to dilute the CO_2 inside the CQ. As we can observe from this figure, CO_2 accumulates in a region which is poorly ventilated and prone to air stagnation. To resolve this problem, it is necessary to adjust, or to help the general ventilation currently in place, with a local ventilation solution. Changing the direction of the ventilation jet in order to affect the central region could produce an uncomfortable sensation of draft for the astronaut. A personalized ventilation solution in parallel to a general one, could be used to redirect a small amount of air towards the region in front of the occupant's face ensuring a supply of fresh air to the area influenced by the breath.

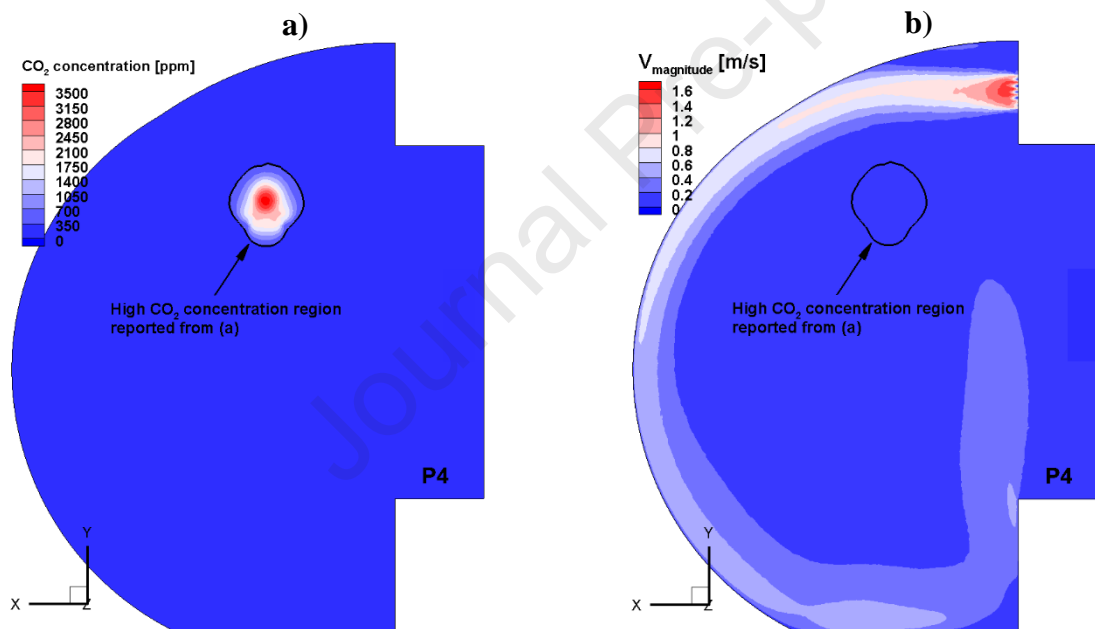


Figure 14 CO_2 concentration as evidenced in [25] (a) superposed over the velocity magnitude fields in P4 (b).

5. Conclusions and future research directions

The current paper proposed an extended study of the general ventilation system of the CQ aboard the ISS via CFD results obtained for the full-scale mock-up, validated through reduced-scale experiments performed in a different working fluid (water), based on similitude criteria.

The first numerical model in the current paper showcases the option of using fan operating curves as boundary conditions to generate realistic inlet velocity distribution of a ventilating jet. To the best of the author's knowledge this procedure is original in the domain of HVAC. The boundary condition most often used in CFD is a velocity profile at the inlet diffuser either constant or experimentally measured beforehand. In order to obtain a high accuracy, these experimental measurements become very complex and expensive. If simulating the ventilation circuit up to the room is

a viable option, then measuring the fan operating curve for use as a boundary condition can be a good alternative to velocity profile measurements.

The second numerical model without the ventilation circuit, which uses an imposed inlet velocity distribution from the first model, was successfully validated using PIV measurements performed in a reduced-scale model. This study was possible by the careful crafting of the reduced-scale mock-up to replicate as best as possible the details of the full-scale mock-up, itself in accord with the details of the real circuit on the ISS. The ventilation circuit with all of its bends and guide vanes, as well as the inlet diffuser grille were reproduced in the reduced-scale mock-up as accurately as the manufacturing process allowed. Using a Reynolds-number based similitude criteria, a close similarity was possible between the water flow in the reduced-scale mock-up and the isothermal airflow in the numerical model. The isothermal conditions imposed in the experimental and the numerical models were aimed at cancelling the effects of gravity to render certain similarity criteria valid.

The comparison between the numerical and PIV measurements shows that the recirculation of the air inside the CQ is highlighted in both cases, creating an air stagnation zone in the centre of the model. The velocity profiles along the curved wall of the CQ have been superposed between the two cases and were found to be in good agreement.

The purpose of this study, to numerically reproduce the general ventilation inside the CQ using a fan operating curve as a boundary condition, was accomplished and lends confidence in the use of the current numerical model in future studies. A preliminary comparison with the authors previous work highlights the weak potential of the current ventilation solution to ventilate the centre of the CQ where the human occupants rest. Future research will focus on investigating alternative ventilation options to improve ventilation in the stagnant air region.

Acknowledgements

This work was supported by a “Presidency” scholarship from the University of Rennes 1, for which the authors are grateful.

This work was also supported by the grant of the Romanian Space Agency ROSA STAR-CDI-C3-2016-577.

References

- [1] NASA, National Aeronautics and Space Administration HUMAN INTEGRATION DESIGN HANDBOOK, Spaceflight (Lond). (2010) 1–27. <https://doi.org/NASA/SP-2010-3407>.
- [2] J.T. James, The headache of carbon dioxide exposures, SAE Tech. Pap. (2007). <https://doi.org/10.4271/2007-01-3218>.
- [3] C.M. Matty, Overview of Carbon Dioxide Control Issues During International Space Station/Space Shuttle Joint Docked Operations, 40th Int. Conf. Environ. Syst. 2 (2010) 1–9. <https://doi.org/10.2514/6.2010-6251>.
- [4] J.T. James, V.E. Meyers, W. Sipes, R.R. Scully, C.M. Matty, Crew Health and Performance Improvements with Reduced Carbon Dioxide Levels and the Resource Impact to Accomplish Those Reductions, (2011) 1–7.
- [5] S. Fairburn, S. Walker, ‘Sleeping With the Stars’ – The Design of a Personal Crew Quarter for the International Space Station, in: 31st Int. Conf. Environ. Syst., 2001. <https://doi.org/10.4271/2001-01-2169>.
- [6] J.L. Broyan, M.A. Borrego, J.F. Bahr, International Space Station USOS Crew Quarters Development, 38th Int. Conference Environ. Syst. (2008). <https://doi.org/10.4271/2008-01-2026>.
- [7] J. Constantinide, H. Najafi, Present state and future of environmental control systems in space, ASHRAE J. 62

(2020) 12–16.

- [8] J. Broyan, D. Welsh, S. Cady, International Space Station Crew Quarters Ventilation and Acoustic Design Implementation, 40th Int. Conf. Environ. Syst. (2010) 1–16. <https://doi.org/10.2514/6.2010-6018>.
- [9] T.P. Schlesinger, B.R. Rodriguez, International Space Station Crew Quarters On-Orbit Performance and Sustaining Activities, Int. Conf. Environ. Syst. (2013) 1–9. <https://doi.org/10.2514/6.2013-3515>.
- [10] J.L. Broyan Jr, M.A. Borrego, J.F. Bahr, International Space Station United States Operational Segment Crew Quarters On-orbit vs. Design Performance Comparison, SAE Int. J. Aerosp. 4 (2011) 98–107. <https://doi.org/10.4271/2009-01-2367>.
- [11] D. Law J., Watkins S., Alexander, W.S. Law J., In-Flight Carbon Dioxide Exposures and Related Symptoms: Associations, Susceptibility and Operational Implications, NASA Tech. Rep. (2010) 1–21. <https://doi.org/NASA/TP-2010-216126>.
- [12] G. Chitaru, C. Croitoru, M. Sandu, I. Nastase, F. Bode, A. Dogeanu, Optimization process for an industrial ventilation system installed inside a sludge dehydration hall, Proc. 2019 Int. Conf. ENERGY Environ. CIEM 2019. (2019) 434–438. <https://doi.org/10.1109/CIEM46456.2019.8937576>.
- [13] M.R. Georgescu, I. Nastase, A. Meslem, M. Sandu, F. Bode, Design of a small-scale experimental model of the international space station crew quarters for a PIV flow field study, E3S Web Conf. 111 (2019). <https://doi.org/10.1051/e3sconf/201911101045>.
- [14] A. Li, P. Tao, X. Bao, Y. Zhao, PIV measurements of air distribution in a reduced-scale model - Ventilation of a busbar corridor in a hydropower station, Int. J. Vent. 12 (2013) 81–98. <https://doi.org/10.1080/14733315.2013.11684004>.
- [15] T. van Hooff, B. Blocken, T. Defraeye, J. Carmeliet, G.J.F. van Heijst, PIV measurements and analysis of transitional flow in a reduced-scale model: Ventilation by a free plane jet with Coanda effect, Build. Environ. 56 (2012) 301–313. <https://doi.org/10.1016/j.buildenv.2012.03.020>.
- [16] T. Lin, O.A. Zargar, K.Y. Lin, O. Juiña, D.L. Sabusap, S.C. Hu, G. Leggett, An experimental study of the flow characteristics and velocity fields in an operating room with laminar airflow ventilation, J. Build. Eng. 29 (2020) 1–9. <https://doi.org/10.1016/j.jobbe.2020.101184>.
- [17] M.Z.I. Bangalee, J.J. Miao, S.Y. Lin, J.H. Yang, Flow visualization, PIV measurement and CFD calculation for fluid-driven natural cross-ventilation in a scale model, Energy Build. 66 (2013) 306–314. <https://doi.org/10.1016/j.enbuild.2013.07.005>.
- [18] J.M. Lirola, E. Castañeda, B. Lauret, M. Khayet, A review on experimental research using scale models for buildings: Application and methodologies, Energy Build. 142 (2017) 72–110. <https://doi.org/10.1016/j.enbuild.2017.02.060>.
- [19] S.B. Wibowo, Sutrisno, T.A. Rohmat, Z. Anwar, F.R. Syadi, R. Mahardika, W.F. Naufal, An investigation into the use of GAMA water tunnel for visualization of vortex breakdown on the delta wing, AIP Conf. Proc. 2001 (2018). <https://doi.org/10.1063/1.5049998>.
- [20] L.P. Erm, M. V Ol, An Assessment of the Usefulness of Water Tunnels for Aerodynamic Investigations, Air Veh. Div. Def. Sci. Technol. Organ. - Aust. (2012) 38. <http://dspace.dsto.defence.gov.au/dspace/%0A15>.
- [21] W. Moog, Room flow tests in a reduced scale., in: ASHRAE Trans. ISSN 0001-2505; USA;, 1981: pp. 1162–1181.
- [22] T. Van Hooff, B. Blocken, T. Defraeye, J. Carmeliet, G.J.F. Van Heijst, PIV measurements of a plane wall jet in a confined space at transitional slot Reynolds numbers, Exp. Fluids. 53 (2012) 499–517. <https://doi.org/10.1007/s00348-012-1305-5>.
- [23] X. Cao, J. Liu, J. Pei, Y. Zhang, J. Li, X. Zhu, 2D-PIV measurement of aircraft cabin air distribution with a high spatial resolution, Build. Environ. 82 (2014) 9–19. <https://doi.org/10.1016/j.buildenv.2014.07.027>.

- [24] X. Cao, J. Li, J. Liu, W. Yang, 2D-PIV measurement of isothermal air jets from a multi-slot diffuser in aircraft cabin environment, *Build. Environ.* 99 (2016) 44–58. <https://doi.org/10.1016/j.buildenv.2016.01.018>.
- [25] M.R. Georgescu, A. Meslem, I. Nastase, Accumulation and spatial distribution of CO₂ in the astronaut's crew quarters on the International Space Station, *Build. Environ.* 185 (2020) 107278. <https://doi.org/10.1016/j.buildenv.2020.107278>.
- [26] C.P. Coutinho, A.J. Baptista, J. Dias Rodrigues, Reduced scale models based on similitude theory: A review up to 2015, *Eng. Struct.* 119 (2016) 81–94. <https://doi.org/10.1016/j.engstruct.2016.04.016>.
- [27] A.-M. Georgescu, S.-C. Georgescu, M. Degeratu, S. Bernad, C.I. Cosoiu, Numerical Modelling Comparison between Airflow and Water Flow within the Achard-Type Turbine, *Sci. Bull. Politeh. Univ. Timișoara, Trans. Mech.* (ISSN 1224-6077). vol 52(66) (2007) 289–298.
- [28] E. Szűcs, *Fundamental Studies in Engineering - Similitude and Modelling*, Elsevier, 1980.
- [29] P. Danca, F. Bode, I. Nastase, A. Meslem, On the Possibility of CFD Modeling of the Indoor Environment in a Vehicle, *Energy Procedia.* 112 (2017) 656–663. <https://doi.org/10.1016/j.egypro.2017.03.1133>.
- [30] M. Darvish, S. Frank, toward the CFD simulation of Sirocco fans: From selecting a Turbulence Model to the role of Cell Shapes, *Int. Conf. Fan Noise, Technol. Numer. Methods (FAN 2012)*, Senlis, Fr. April. (2012) 18–20.
- [31] J. Tamminen, T. Ahonen, J. Ahola, S. Hammo, Fan pressure-based testing, adjusting, and balancing of a ventilation system, *Energy Effic.* 9 (2016) 425–433. <https://doi.org/10.1007/s12053-015-9372-0>.
- [32] I. Kohri, Y. Kobayashi, Y. Matsushima, Prediction of the Performance of the Engine Cooling Fan with CFD Simulation, *SAE Int. J. Passeng. Cars - Mech. Syst.* 3 (2010) 508–522. <https://doi.org/10.4271/2010-01-0548>.
- [33] F. Pérot, M.S. Kim, S. Moreau, D. Neal, Investigation of the flow generated by an axial 3-blade fan, 13th Int. Symp. Transp. Phenom. Dyn. Rotating Mach. 2010, ISROMAC-13. (2010) 198–204.
- [34] ANSYS Fluent Theory Guide, ANSYS Fluent Theory Guide, ANSYS Inc., USA. 15317 (2013) 724–746. http://www.afs.enea.it/project/neptunius/docs/fluent/html/th/main_pre.htm.
- [35] A.-M. Georgescu, S.-C. Georgescu, Simplified Numerical Model of an Axial Impeller, 2012 COMSOL Conf. (2012) 1–4.
- [36] C. Meyer, D.G. Kroger, A Numerical investigation of the errors associated with the scaling of axial flow fan performance characteristics, *R D J.* (2004).
- [37] F.N. Le Roux, *The CFD simulation of an axial flow fan*, Thesis. (2010).
- [38] S.J. Van Der Spuy, T.W. Von Backström, An evaluation of simplified CFD models applied to perimeter fans in air-cooled steam condensers, *Proc. Inst. Mech. Eng. Part A J. Power Energy.* 229 (2015) 948–967. <https://doi.org/10.1177/0957650915594073>.
- [39] C. Croitoru, I. Nastase, A. Iatan, V. Iordache, A. Meslem, Numerical and experimental modeling of airflow and heat transfer of a human body, (2011). https://scholar.google.com/scholar?hl=en&as_sdt=0,5&cluster=11950048267351706237 (accessed February 8, 2019).
- [40] P. Danca, F. Bode, I. Nastase, A. Meslem, CFD simulation of a cabin thermal environment with and without human body – thermal comfort evaluation, *E3S Web Conf.* 32 (2018) 01018. <https://doi.org/10.1051/e3sconf/20183201018>.
- [41] H. Awbi, *Ventilation of Buildings*, 2nd ed., 2003.

Highlights

- Astronaut comfort during sleep depends on the good ventilation of the crew quarters
- Airflow inside the crew quarters is studied in a reduced-scale model on Earth
- Particle Image Velocimetry techniques are used to obtain the flow fields
- Experimental results are used to validate a CFD model
- Regions susceptible to carbon dioxide accumulation are identified

Journal Pre-proof

Declaration of interests

The authors declare that they have no known competing financial interests or personal relationships that could have appeared to influence the work reported in this paper.

The authors declare the following financial interests/personal relationships which may be considered as potential competing interests:

Matei-Razvan GEORGESCU



Amina MESLEM



Ilinca NASTASE



Mihnea SANDU

